Bulletin of the Seismological Society of America, Vol. 103, No. 4, pp. 2474–2481, August 2013, doi: 10.1785/0120120255

Refined Rupture-Velocity Estimation of the 2009 L'Aquila Earthquake (M_w 6.3, Central Italy) Derived from Apparent Source Time Functions

by Antonella Orefice, Martin Vallée,* Julien Balestra, Bertrand Delouis, and Aldo Zollo

Abstract In this paper, we obtain an accurate estimation of the rupture velocity of the 6 April 2009 M_w 6.3 L'Aquila earthquake (Central Apennines) by analyzing its apparent source time functions (ASTFs). These ASTFs have been extracted by deconvolving an empirical Green's function (EGF) at seismic stations located 200–800 km from the earthquake. From the study of duration, shape, and directivity of ASTFs at numerous and well-distributed stations, we show that the area between the two main slip patches of the earthquake ruptured at a relatively slow velocity (1.6 km/s). We next validate simultaneously the ASTFs and the slip model independently obtained through the joint inversion of strong-motion, broadband teleseismic, Global Positioning System, and Interferometric Synthetic Aperture Radar data. The good agreement in shape and duration between the observed and theoretical ASTFs is an indication for the reliability of the inferred source model and for the robustness of the rupture velocity estimations of this study.

Introduction

The 2009 M_w 6.3 L'Aquila earthquake occurred in the Central Apennines (Italy) on 6 April at 01:32 UTC, with the hypocenter located at 42.35° N, 13.38° E, and at a depth of 9.5 km (Cirella *et al.*, 2009). The earthquake caused nearly 300 casualties, and heavy damage in the town of L'Aquila and in several villages nearby. The mainshock was preceded by a seismic sequence starting a few months before and culminating with an M_L 4.1 event on 30 March 2009, followed by M_L 3.9 and M_L 3.5 foreshocks on 5 April 2009 occurring a few hours before the mainshock. The earthquake rupture developed along a northwest–southeast active segment of a complex normal fault system embedded in the mountain front of the central Apennines chain (Cirella *et al.*, 2009; Walters *et al.*, 2009).

The central Apennines belt belongs to the Mesozoic carbonate platform domain, which is dominated by the rollback of the Adriatic subduction toward the east (Doglioni *et al.*, 1998). This region shows an arclike seismicity distribution in the upper crust that follows the topographic trend. It is generally characterized by normal faults oriented along preexisting compressive tectonic structures (Bigi *et al.*, 2002). Northwest–southeast-striking segments are likely causative for the largest past seismic events (Di Bucci *et al.*, 2010), which are mainly related to normal-faulting mechanisms, consistent with a regional northeast–southwest-trending extensional regime (Selvaggi, 1998; Montone *et al.*, 1999; Serpelloni *et al.*, 2005; Devoti *et al.*, 2008; D'Agostino *et al.*, 2009) and likely controlled by deep crustal-scale detachments (Bigi *et al.*, 2002).

The goal of this work is to infer the rupture kinematic properties of the 6 April 2009 M_w 6.3 L'Aquila earthquake (Central Apennines), based on the analysis and modeling of the apparent source time functions (ASTFs) retrieved from regional waveform data. The ASTFs are calculated by deconvolution of records from a smaller-sized event at the same receivers, using the so-called empirical Green's function (EGF) method (Hartzell, 1978). We here use the deconvolution technique of Vallée (2004), which imposes four physical constraints on the ASTFs in the deconvolution process: causality, positivity, limited duration, and equal area. For any ASTF, its area represents the scalar moment of the earthquake and therefore it has to remain constant at all stations.

The smaller earthquake has to be similar in terms of location and mechanism (typically 1–2 magnitude units smaller than the larger one) so that its waveforms act as the medium transfer functions between the source and the receivers. As the path, site, and instrument effects are similar for both large and small earthquake, the deconvolution of the two earthquake records gives the ASTFs of the larger earthquake at each considered station. The duration and shape of each ASTF can then be examined to infer the extended source properties of the mainshock, such as the rupture extent, the slip distribution, and the rupture velocity.

*Now at Laboratoire de Sismologie, Institut de Physique du Globe de Paris 1 Rue Jussieu, 75238 Paris Cedex 05, France.

Table 1
Hypocentral Coordinates and Focal Mechanism for the Mainshock and EGF

	Origin Time (hh:mm:ss.sss)	Latitude (°)	Longitude (°)	Depth (km)	Strike (°)	Dip (°)	Rake (°)
Mainshock	01:32:40.400	42.342	13.380	8.3	147; 324	43; 47	−88; −92
EGF	09:26:28.620	42.336	13.387	9.6	137; 333	56; 35	−99; −77

Data

After visual inspection of regional (distance 200–800 km) records from several aftershocks in the magnitude range 4–5, we select as EGF an M_w 4.9 aftershock, which occurred on 7 April 2009 at 09:26:29 UTC. This selection provides an optimal signal-to-noise ratio. The differences in focal mechanism and location between the EGF and master event are small (Table 1) and can be considered as negligible when analyzing regional data. The waveforms of 49 broadband stations (Table 2) have been retrieved for the two events from the data servers of the following networks: MedNet (MN), ISNet (IN), INGV (IV), GEOFON (GE), French Broadband Seismological Network (FR), Austrian Seismic Network (OE), Aristotle University of Thessaloniki Seismological AUTH (HT), Slovenia (SL), BayernNetz, Germany (BW), and Hungarian Seismological Network (HU). These stations are located in the distance range 200–800 km and cover the full azimuth range (maximum gap of about 60°; see Fig. 1 and Table 2). At these regional distances, the surface waves are dominant and they suffer less from the contamination of secondary and multipath arrivals than body waves. We therefore apply the deconvolution process to the surface Love- and Rayleigh-wave packets, windowed on the transverse and vertical component, respectively, and filtered between 0.05 and 1 Hz (Fig. 2). The optimal time window is chosen through a visual inspection of waveforms to avoid the presence of secondary phases. The duration of the window is on the order of a few tenths of a second (Fig. 2), thus significantly larger than the durations of the ASTFs, which are in the range 5–10 s. These long time windows ensure the determination of reliable ASTFs.

The deconvolution method of Vallée (2004) is based on the approach of Bertero *et al.* (1997), who developed a simple method to include positivity and temporal constraints on the ASTFs, based on the Landweber method. Calling U^1 and U^0 the mainshock and EGF waveforms, respectively, the problem is to identify the ASTF F_θ verifying $\|U^0 * F_\theta - U^1\| =$ minimum. This optimization is made by the Landweber method, using a relaxation parameter τ equal to $1.5/(\sup_\omega |U^1(\omega)|)^2$. More details on the procedure can be found in Vallée (2004) and Bertero *et al.* (1997). For each station, the misfit between the real (U^1) and the reconstituted ($U^0 * F_\theta$) mainshock waveforms is evaluated in the Love and Rayleigh window. The reconstituted mainshock and its associated misfit are calculated for increasing values of the allowed duration of the ASTF. The misfit evolution as a function of ASTF duration usually takes the shape of an *L* curve and is a good indicator of the quality of the obtained deconvolution. The time at which the function becomes flat gives the simplest (i.e., shortest) ASTF able to well describe the seismic source. If this flat level further corresponds to low values of misfit (~0.3 or lower), the simplest ASTFs are selected for the following analysis of the source process.

Application and Results

Figure 3 shows the ASTFs obtained for all the considered stations with increasing azimuth from left top to right bottom. The presence of two peaks in the ASTFs is clear, as well as the effects of directivity, denoted by the variations of the duration and shape of the ASTFs as a function of azimuth. Qualitative observations of these variations confirm the southeast propagation of the rupture (Maercklin *et al.*, 2011), as stations close to azimuth N140°E (e.g., AND3, CLT3) exhibit the shortest durations and largest amplitudes, while stations in the opposite azimuths (e.g., DAVA, RETA) show the longest durations and smallest amplitudes. This behavior is also visible when focusing on the two peaks of the ASTFs: when moving from stations with directions opposite to the rupture propagation (e.g., station ROBS, azimuth N2°E) to stations along the direction of rupture propagation (e.g., station COL3, azimuth N137°E), we observe that the time interval between the two peaks becomes shorter and that their amplitudes increase. The two peaks of the ASTFs can thus be associated to distinct high-slip zones activated during the southeast propagation of the rupture, and whose relative distance and rupture velocity control the time interval. The evidence for two main high-slip patches controlling the rupture process of the 2009 L'Aquila earthquake is confirmed by the kinematic rupture modeling using different data sets (Cirella *et al.*, 2009, 2012; J. Balestra and B. Delouis, personal comm., 2012).

In order to get an estimation of the distance *L* and average rupture velocity V_r between the two high-slip patches, we measure the difference $\Delta\tau$ between the arrival times of first and second peak on all the ASTFs. According to the kinematic source models retrieved for the L'Aquila event from near-source and regional strong-motion data, Global Positioning System (GPS) data, and Interferometric Synthetic Aperture Radar (InSAR) images (e.g., Cirella *et al.*, 2009; Maercklin *et al.*, 2011), we assume a Haskell-type source model (Haskell, 1969) with a unilateral rupture propagating along the direction 137°. In this case, we have

$$\Delta\tau = \frac{L}{V_r}\left(1 - \frac{V_r}{c}\cos\alpha\right), \tag{1}$$

Table 2
Station Code, Location, and Seismic Network of the Stations Used in This Study

Station Code	Latitude (°)	Longitude (°)	Elevation (m)	Azimuth (°)	Network
ROBS	46.24	13.51	245.0	2.2	SL
MYCA	46.63	13.64	909.0	3.2	OE
CADS	46.23	13.74	751.0	4.5	SL
TRI	45.71	13.74	161.0	5.6	MN
MOA	47.85	14.27	572.0	6.8	OE
JAVS	45.89	14.06	1100.0	8.7	SL
OBKA	46.51	14.55	1075.0	11.8	OE
CEY	45.74	14.42	579.0	13.2	SL
LJU	46.04	14.53	396.0	13.2	SL
KNDS	45.53	14.38	1035.0	13.6	SL
SOKA	46.68	15.03	1008.5	15.6	OE
PERS	46.64	15.11	795.0	16.4	SL
VISS	45.80	14.84	399.0	17.5	SL
ARSA	47.25	15.52	577.0	17.3	OE
CSNA	47.93	15.86	1039.0	17.2	OE
GROS	46.46	15.50	930.0	20.5	SL
SOP	47.68	16.56	260.0	22.5	HU
CRES	45.83	15.46	433.0	23.7	SL
PKSM	46.21	18.64	170.0	43.3	HU
DIVS	44.10	19.99	1000.0	68.6	MN
PDG	42.43	19.26	40.0	87.6	MN
FNA	40.78	21.38	750.0	102.2	HT
NOCI	40.79	17.06	420.0	118.4	IV
MATE	40.65	16.70	494.0	123.2	GE
AVG3	40.76	15.72	1213.0	130.4	IN
CLT3	40.90	15.40	525.0	132.0	IN
BEL3	40.72	15.64	758.0	132.3	IN
AND3	40.93	15.33	905.0	132.4	IN
RSF3	40.96	15.18	865.0	134.1	IN
STN3	40.53	15.65	832.0	135.2	IN
CGG3	40.54	15.52	1067.0	136.7	IN
COL3	40.69	15.33	1026.0	137.0	IN
NSC3	40.85	15,12	1300.0	137.3	IN
SNR3	40.74	15.19	1009.0	138.2	IN
SRN3	40.49	15.46	1067.0	138.4	IN
MNT3	40.84	15.01	866.0	139.4	IN
PST3	40.56	15,24	762.0	140.4	IN
CUC	39.99	15.81	637.0	140.9	MN
CMP3	40.65	15.08	958.0	141.4	IN
CEL	38.26	15.89	702.0	153.5	MN
WDD	35.87	14.52	41.0	171.3	MN
VSL	39.50	9.38	370.0	227.0	MN
ISO	44.18	7.05	910.0	293.5	FR
BNI	45.05	6.68	1395.0	301.2	MN
VLC	44.16	10.39	555.0	310.6	MN
DAVA	47.29	9.88	1602.0	334.7	OE
RETA	47.49	10.76	965.0	341.4	OE
RJOB	47.74	12.80	860.0	356.3	BW
KBA	47.08	13.34	1721.0	0.4	OE

See also the map in Figure 1. The station list is ordered by azimuth.

where c is the phase velocity of the wave used in the deconvolution process, and α is the directivity angle between the rupture direction and the surface-wave propagation direction. For this analysis we only use the ASTFs calculated from the mainshock and EGF transverse signals in the Love-wave time window. The quality of the deconvolutions is generally higher for Love waves than for Rayleigh waves, and the use of Love waves alone allows us to obtain a good azimuthal coverage. The addition of Rayleigh waves would therefore provide very little supplemental information but would make the analysis more complex, because of the introduction of another phase velocity. The Love-wave phase velocity is set equal to 3.9 km/s according to the study of Ekström (2011). By a nonlinear fitting of the observed data $\Delta\tau$ adopting the theoretical model in equation (1), we determine an interpatch rupture velocity V_r equal to 1.60 ($\pm$0.04) km/s and an interpatch distance L equal to 4.9 ($\pm$0.3) km (dashed curve in Fig. 4). We apply the nonlinear Levenberg–Marquardt least-square algorithm (Marquardt, 1963), implemented in the software package gnuplot (Janert, 2009) for curve fitting and parameters estimation. The estimated value of V_r corresponds to about 50%–60% of the shallow crustal shear-wave velocity at the depth of the source according to Bagh *et al.* (2007). In order to test the robustness of this rupture velocity, we show in Figure 4 the optimal models corresponding to faster rupture velocities and the variation of root mean square (rms) of residuals for the different models. This shows that rupture velocities V_r faster than 2 km/s do not well explain the apparent durations; in fact, the values of the rms of residuals increases with V_r. This relatively slow rupture propagation is consistent with results from kinematic inversion models obtained by the combined inversion of teleseismic, accelerometer, and GPS data (J. Balestra and B. Delouis, personal comm., 2012; Yano *et al.*, 2009). Cirella *et al.* (2009) found a distance between patches of about 9 km and an associated rupture velocity on the order of 2 km/s. However, a more recent study (Cirella *et al.*, 2012) indicates a slower rupture velocity (1.5–2 km/s) and shorter distance between patches (7 km), in closer agreement with our results.

In this study, we want to validate simultaneously the ASTFs and the slip model independently obtained by J. Balestra and B. Delouis (personal comm., 2012). This model is obtained from the joint inversion of strong-motion, broadband teleseismic, GPS, and InSAR data. The method is based on a parameterization allowing for variable slip and variable-rupture velocity (Delouis *et al.*, 2002). The approach combines the multiple time-windows formulation (Olson and Aspel, 1982; Hartzell and Heaton, 1983) with a nonlinear inversion solved by simulated annealing. Convergence is based on the minimization of an rms misfit function and total seismic moment. The preferred fault geometry is a single fault segment striking N137°, dipping 45° southwest, with an average rake of −105°. Model dimensions are 24 km along strike and 18 km along dip. The segment is divided into 192 square subfaults measuring 1.5 km along strike and dip. Each subfault is considered as a point source associated with a local source time function represented by three isosceles triangular functions. The total width of each function is 1 s, and the three functions are mutually overlapping. The free parameters for which inversions were done are the rupture onset time, the rake, and the amplitude of the triangular functions, at each subfault. The rupture velocity is allowed to vary between 1.0 and 2.5 km/s.

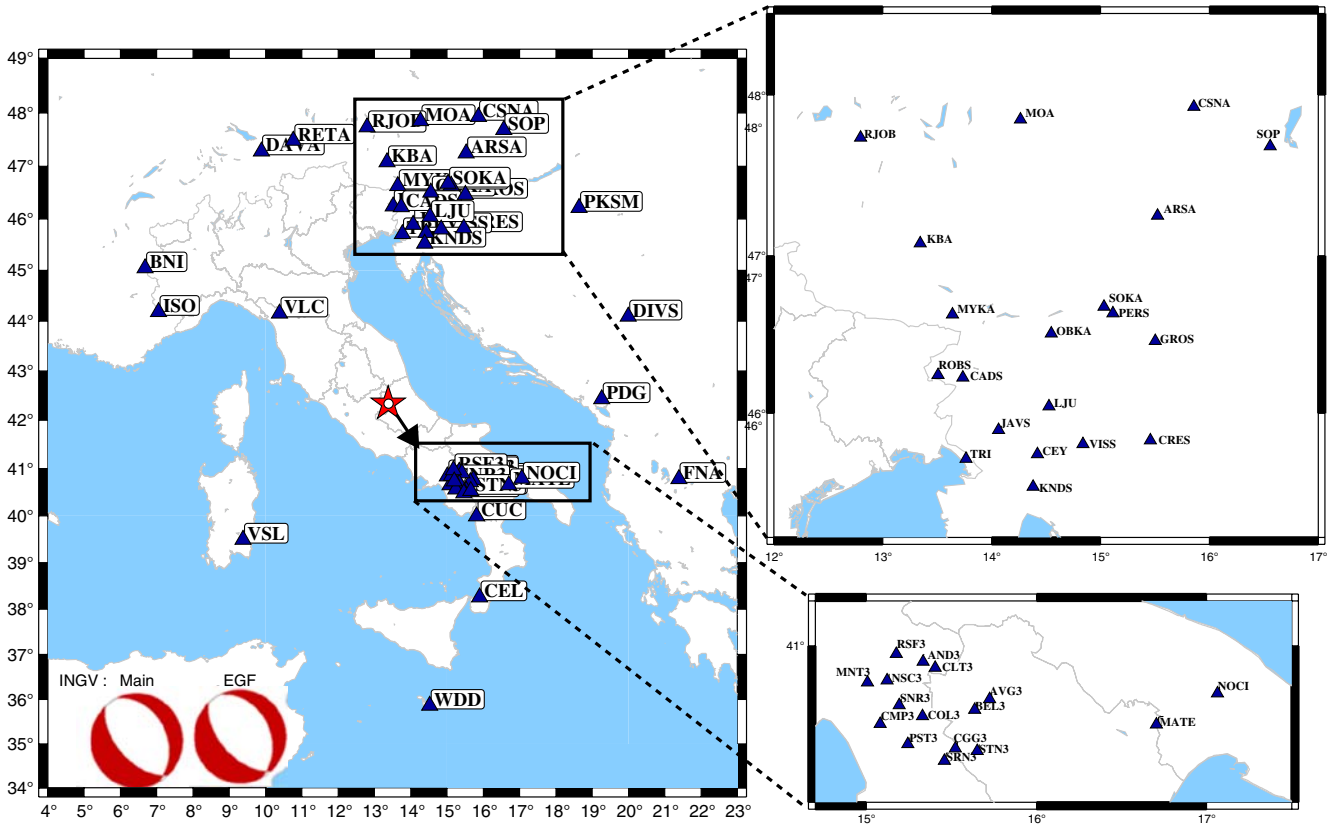

Figure 1. Map of seismic stations used in this study. The location of the M_w 6.3 mainshock (star) and EGF (circle almost collocated with the star) are also shown. The arrow indicates the rupture direction of the mainshock (Maercklin *et al.*, 2011). The color version of this figure is available only in the electronic edition.

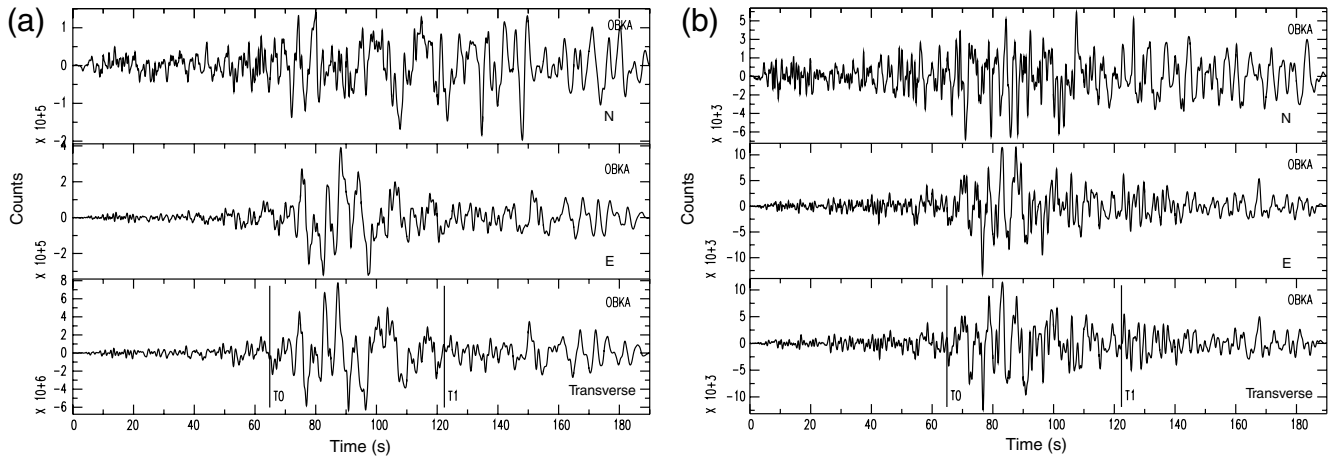

Figure 2. Example of Love-wave time windows [T0 T1] at station OBKA. (a, b) Shows the velocity components of the mainshock and EGF, respectively. The waveforms are filtered in the range of frequencies used in the deconvolution process (i.e., 0.05–1 Hz). The two horizontal north and east components (upper panels) are rotated along the transverse direction to record the Love waves. The transverse components, windowed in the interval [T0 T1], are used in the deconvolution process.

The top panel of Figure 5 compares the observed (filled curves) and synthetic (dashed curves) ASTFs. The latter have been obtained from the source model resulting from the joint inversion (bottom panel of Fig. 5), by integrating the subfault source functions with the appropriated spatial and temporal shifts (e.g., equation 6 in Vallée *et al.*, 2011). In Figure 5, only slip values greater than 15% of the maximum slip (130 cm) are represented. The slip map shows two main slip

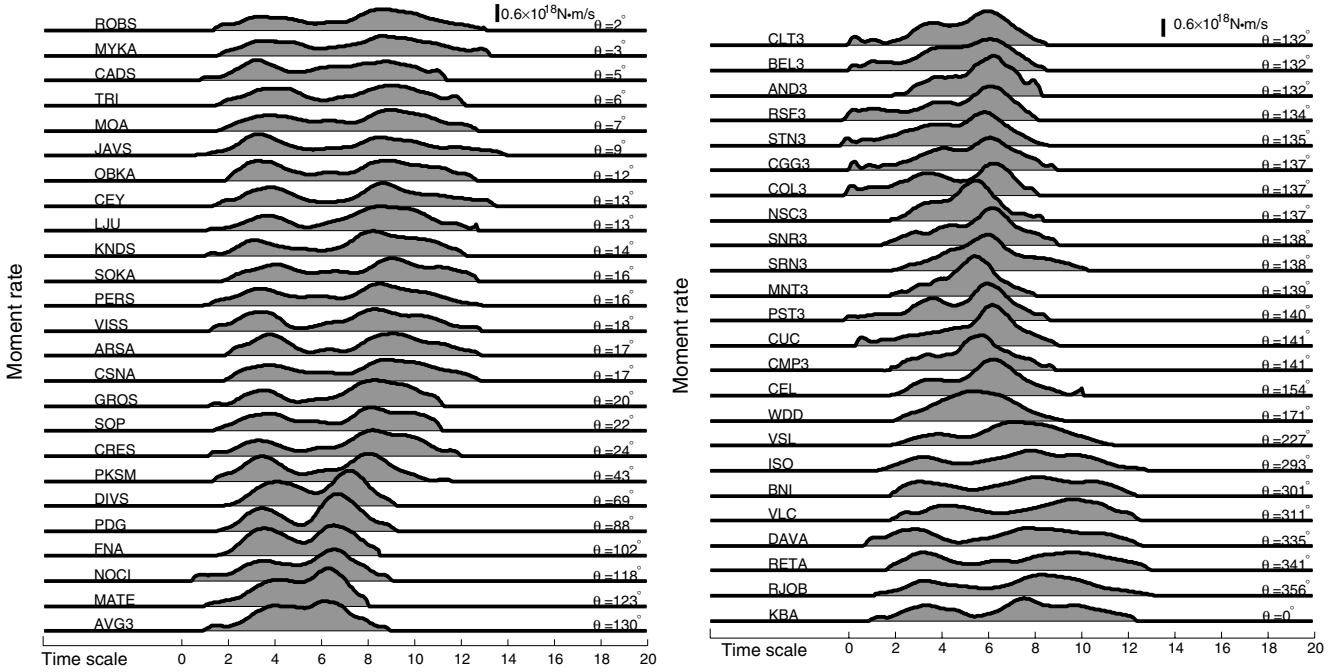

Figure 3. ASTFs of M_w 6.3 L'Aquila mainshock, obtained by stabilized deconvolution. Name and azimuths of the stations are shown to the left and right of each ASTF, respectively. All ASTFs are shown at the same scale (indicated by the vertical bar at the top of the figure) and ordered by azimuth.

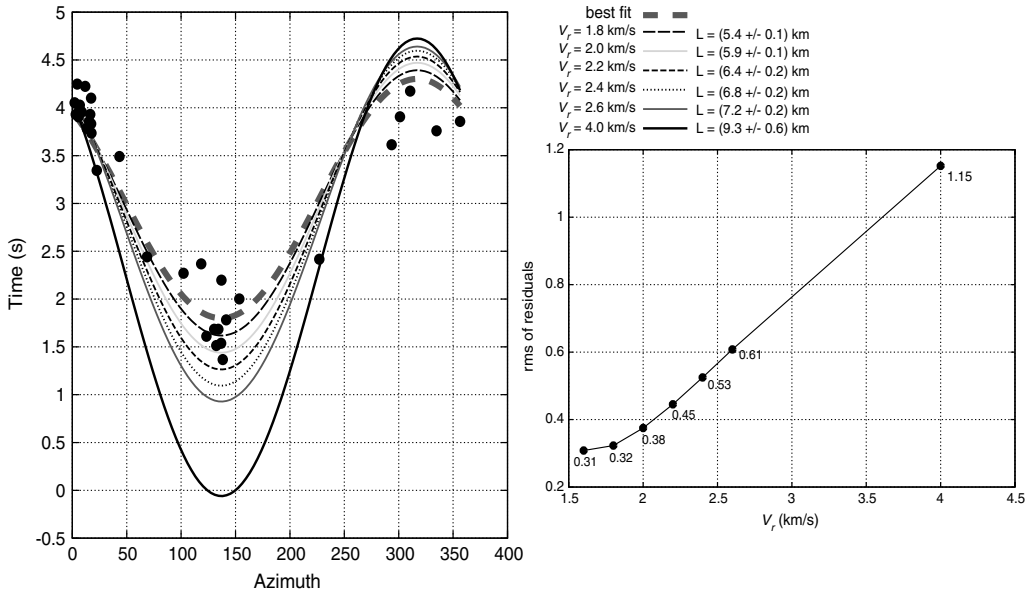

Figure 4. Fit between the observed apparent durations (solid circles) and the ones corresponding to the optimal unilateral model (bold dashed curve). The observed data are the differences between the apparent times of the first and second bumps. The other curves were obtained by fixing the rupture velocity V_r to the values indicated in the right part of the figure. For each value of V_r the estimated value of L is reported. In the right part of this figure the variation of rms of residuals is also shown for each value of V_r. It increases with V_r from 0.31 (best model, i.e., $V_r = 1.6$ km/s) to 1.15 ($V_r = 4.0$ km/s).

areas. A small one (Z1) is located at and above the hypocenter, and a major one (Z2) is located to the southeast of the hypocenter. The average slip value is about 46 cm for the total rupture area. The average rupture velocity is 1.8 km/s. Onset time curves in Figure 5b show that the delay between the two slip areas Z1 and Z2, separated by 5 km, is about 3 s. This indicates that the rupture propagated between those two zones at a velocity close to 1.67 km/s, in good agreement

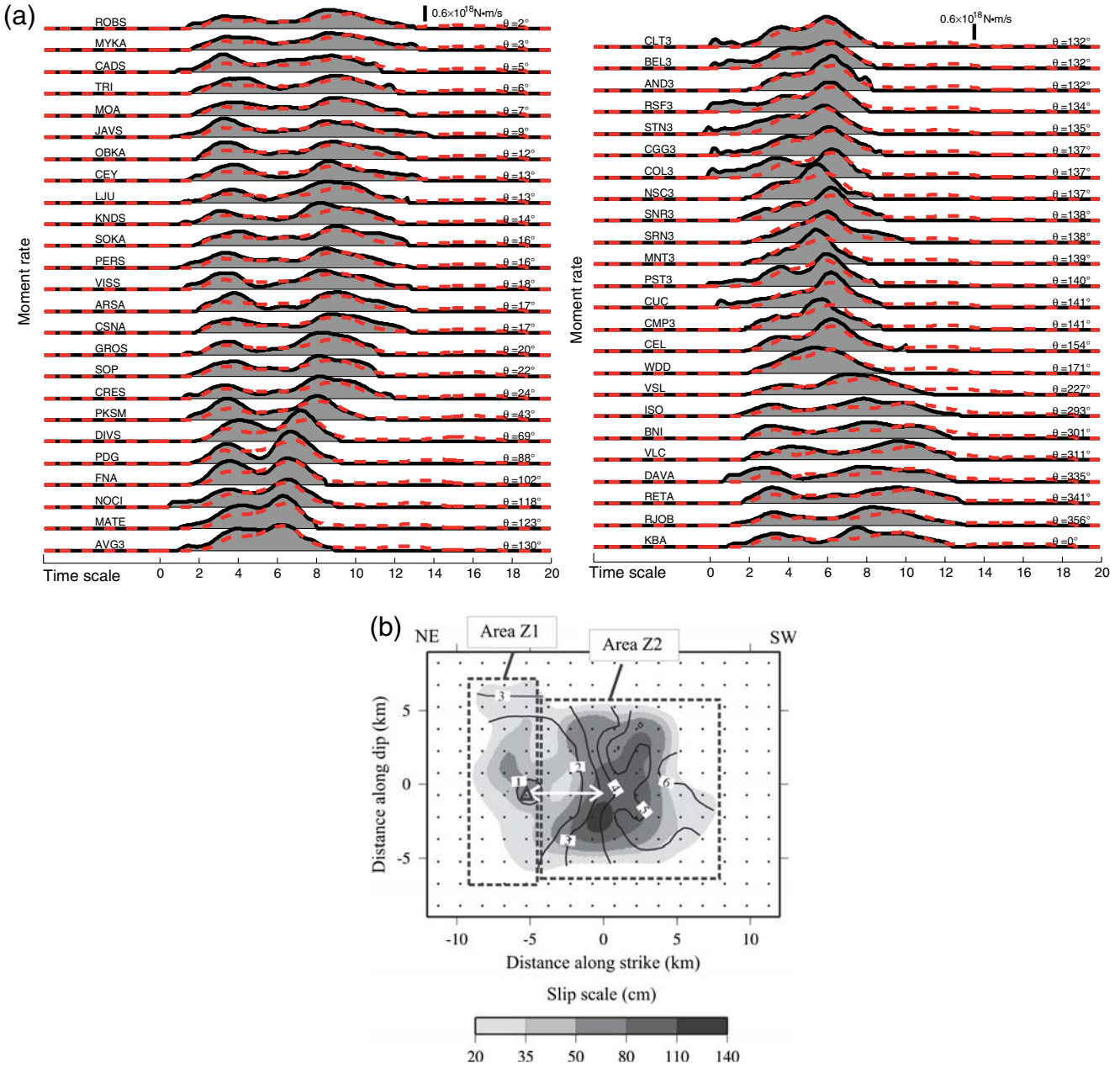

Figure 5. (a) Comparison between observed and computed ASTFs. Observed ASTFs (filled curves) are obtained by the deconvolutive approach. Computed ASTFs (dashed curves) are computed from (b) the rupture process model of J. Balestra and B. Delouis (personal comm., 2012). The triangle in the slip model locates the hypocenter. Black points correspond to individual point sources. Black continuous lines and their associated labels indicate rupture onset time in seconds. Dashed rectangles show the two main slip areas Z1 and Z2. The double arrow shows that the horizontal distance between the two asperities is of order of 5 km, in agreement with the results of analysis of ASTFs. The delay between the two slip areas Z1 and Z2 is about 3 s, as indicated by the onset time curves. The color version of this figure is available only in the electronic edition.

with the result of the ASTFs analysis. As concerns the rupture length, our estimation of the distance between high-slip patches ($L = 4.9$ km) well matches the centroid distances (double arrow in slip model) between the asperities revealed by the rupture kinematic modeling. We note that the observed and theoretical ASTFs are very consistent both in shape and duration at all the considered stations, which is an indication for the reliability of the inferred source model and robustness of the rupture-velocity and length estimations of this study.

Conclusion

By applying the EGF approach to broadband regional data, we have obtained the ASTFs of the M_w 6.3 L'Aquila

mainshock (central Apennines). The main results of this study may be summarized in the following points:

1. From the arrival-time difference between the first and second peak on all the ASTFs, we determine that the rupture velocity is equal to (1.60 ± 0.04) km/s. This is the average rupture velocity in the area between the two high-slip patches. Could the relatively slow rupture velocity be associated with presence and migration of fluids? Several studies have demonstrated that fluid flow and/or pore-pressure evolution can affect earthquake ruptures (Bizzarri and Cocco, 2006; Templeton and Rice, 2008; Viesca *et al.*, 2008). Zaccarelli *et al.* (2011) show that the L'Aquila mainshock caused a perceptible decrease of seismic velocities due to an increase of crack and void densities in the shallow crustal structure. Lucente *et al.* (2011) infer that a complex sequence of dilatancy–diffusion processes in the nucleation area are responsible for variation of elastic and anisotropic parameters during the earthquake. In addition, the tomographic results show the presence of low-V_P and high-V_P/V_S anomalies in the hypocentral area, consistent with the presence of fluid-filled rock volumes (Chiarabba *et al.*, 2010; Terakawa *et al.*, 2010; Di Stefano *et al.*, 2011). Then the relatively slow rupture velocity could be due to the presence of heterogeneity on the fault, both in terms of rheological properties and geometrical irregularities (Bizzarri *et al.*, 2010).
2. The two peaks in the ASTFs are an indication that the fracture process was complex, and that slip and/or rupture velocity must necessarily be heterogeneous. This is confirmed by the good agreement between the observed and theoretical ASTFs obtained from the study of J. Balestra and B. Delouis (personal comm., 2012) with independent data. Through the joint inversion of strong-motion, broadband teleseismic, GPS, and InSAR data, J. Balestra and B. Delouis obtain theoretical ASTFs very similar in shape and duration to ASTFs obtained through EGF deconvolution. This similarity independently supports their extended source model and illustrates how the EGF approach is sensitive to details of the rupture process. In the particular case of L'Aquila earthquake, the ASTFs variations offer a robust and straightforward insight into the slow rupture velocity between the hypocentral area and the main slip patch.

Data and Resources

Seismic data used in this study were collected by ISNet (Irpinia Seismic Network) southern Italy network and Orfeus Data Center (ODC; http://www.orfeus-eu.org/Data-info/data.html). The information on location and focal mechanism of seismic data used in this study are taken from the catalogs Italian Seismological Instrumental and Parametric Data-Base (ISIDe, http://iside.rm.ingv.it) and Istituto Nazionale di Geofisica e Vulcanologia (INGV, http://cnt.rm.ingv.it), respectively.

Some of the figures were made using gnuplot (http://www.gnuplot.info/), MATLAB, and Generic Mapping Tools (GMT; www.soest.hawaii.edu/gmt/). Webpages were last accessed on 27 December 2012.

Acknowledgments

We thank the two anonymous reviewers and Associate Editor Arthur McGarr for their comments.

References

Bagh, S., L. Chiaraluce, P. De Gori, M. Moretti, A. Govoni, C. Chiarabba, P. Di Bartolomeo, and M. Romanelli (2007). Background seismicity in the Central Apennines of Italy: The Abruzzo region case study, *Tectonophysics*, **444,** nos. 1–4, 80–92, doi: 10.1016/j.tecto.2007.08.009.

Bertero, M., D. Bindi, P. Boccacci, M. Cattaneo, C. Eva, and V. Lanza (1997). Application of the projected Landweber method to the estimation of the source time function in seismology, *Inverse Probl.* **13,** 465–486.

Bigi, S., C. Doglioni, and G. Mariotti (2002). Thrust vs normal fault decollements in the Central Apennines, *Boll. Soc. Geol. Ital.* **1,** 161–166.

Bizzarri, A., and M. Cocco (2006). A thermal pressurization model for the spontaneous dynamic rupture propagation on a three-dimensional fault: 1. Methodological approach, *J. Geophys. Res.* **111,** B05303, doi: 10.1029/2005JB003862.

Bizzarri, A., E. M. Dunham, and P. Spudich (2010). Coherence of Mach fronts during heterogeneous supershear earthquake rupture propagation: Simulations and comparison with observations, *J. Geophys. Res.* **115,** B08301, doi: 10.1029/2009JB006819.

Chiarabba, C., S. Bagh, I. Bianchi, P. De Gori, and M. Barchi (2010). Deep structural heterogeneities and the tectonic evolution of the Abruzzi region (Central Apennines, Italy) revealed by microseismicity, seismic tomography, and teleseismic receiver functions, *Earth Planet. Sci. Lett.* **295,** nos. 3–4, 462–476, doi: 10.1016/j.epsl.2010.04.028.

Cirella, A., A. Piatanesi, M. Cocco, E. Tinti, L. Scognamiglio, A. Michelini, A. Lomax, and E. Boschi (2009). Rupture history of the 2009 L'Aquila (Italy) earthquake from nonlinear joint inversion of strong motion and GPS data, *Geophys. Res. Lett.* **36,** no. 19, L19304, doi: 10.1029/2009GL039795.

Cirella, A., A. Piatanesi, E. Tinti, M. Chini, and M. Cocco (2012). Complexity of the rupture process during the 2009 L'Aquila, Italy, earthquake, *Geophys. J. Int.* **190,** 607–621, doi: 10.1111/j.1365-246X.2012.05505.x

D'Agostino, N., S. Mantenuto, E. D'Anastasio, A. Avallone, M. Barchi, C. Collettini, F. Radicioni, A. Stoppini, and G. Castellini (2009). Contemporary crustal extension in the Umbria–Marche Apennines from regional CGPS networks and comparison between geodetic and seismic deformation, *Tectonophysics*, **476,** 3–12.

Delouis, B., D. Giardini, P. Lungren, and J. Salichon (2002). Joint inversion of InSAR, GPS, teleseismic, and strong motion data for the spatial and temporal distribution of earthquake slip: Application to the 1999 Izmit mainshock, *Bull. Seismol. Soc. Am.* **92,** 278–299.

Devoti, R., F. Riguzzi, M. Cuffaro, and C. Doglioni (2008). New GPS constraints on the kinematics of the Apennines subduction, *Earth Planet. Sci. Lett.* **273,** 163–174, doi: 10.1016/j.epsl.2008.06.031.

Di Bucci, D., P. Burrato, P. Vannoli, and G. Valensise (2010). Tectonic evidence for the ongoing Africa-Eurasia convergence in central Mediterranean foreland areas: A journey among long-lived shear zones, large earthquakes, and elusive fault motions, *J. Geophys. Res.* **115,** B12404, doi: 10.1029/2009JB006480.

Di Stefano, R., C. Chiarabba, L. Chiaraluce, M. Cocco, P. De Gori, D. Piccinini, and L. Valoroso (2011). Fault zone properties affecting the rupture evolution of the 2009 (M_w 6.1) L'Aquila earthquake (central Italy): Insights from seismic tomography, *J. Geophys. Res.* **38,** L10310, doi: 10.1029/2011GL047365.

Doglioni, C., F. Mongelli, and G. Pialli (1998). Boudinage of the Alpine belt in the Apenninic back-arc, *Mem. Soc. Geol.* **52,** 457– 468.

Ekström, G. (2011). A global model of Love and Rayleigh surface wave dispersion and anisotropy, 25–250 s, *Geophy. J. Int.* doi: 10.1111/j.1365-246X.2011.05225.x

Hartzell, S. H. (1978). Earthquake aftershocks as Green's functions, *Geophys. Res. Lett.* **5,** 1–4.

Hartzell, S. H., and T. H. Heaton (1983). Inversion of strong motion and teleseismic waveform data for the fault rupture history of the 1979 Imperial Valley, California, earthquake, *Bull. Seismol. Soc. Am.* **73,** 1533–1583.

Haskell, N. A. (1969). Elastic displacements in the near-field of a propagating fault, *Bull. Seismol. Soc. Am.* **59,** 865–908.

Janert, K. P. (2009). *Gnuplot in Action: Understanding Data with Graphs*, Manning Publications Co., Greenwich, Connecticut, 396 pp.

Lucente, F. P., P. De Gori, L. Margheriti, D. Piccinini, M. Di Bona, C. Chiarabba, and N. Piana Agostinetti (2011). Temporal variation of seismic velocity and anisotropy before the 2009 M_w 6.3 L'Aquila earthquake, Italy, *Geology* **38,** 1014–1018, doi: 10.1130/G31463.1

Maercklin, N., A. Zollo, A. Orefice, G. Festa, A. Emolo, R. De Matteis, B. Delouis, and A. Bobbio (2011). The effectiveness of a distant accelerometer array to compute seismic source parameters: The April 2009 L'Aquila Earthquake case history, *Bull. Seismol. Soc. Am.* **101,** 354–365.

Marquardt, D. (1963). An algorithm for least-squares estimation of nonlinear parameters, *SIAM J. Appl. Math.* **11,** 431–441, doi: 10.1137/0111030.

Montone, P., A. Amato, and S. Pondrelli (1999). Active stress map of Italy, *J. Geophys. Res.*, **104,** 25,595–25,610, doi: 10.1029/1999JB900181.

Olson, A. H., and R. J. Aspel (1982). Finite fault and inverse theory with applications to the 1979 Imperial Valley earthquake, *Bull. Seismol. Soc. Am.* **72,** 1969–2001.

Selvaggi, G. (1998). Spatial distribution of horizontal seismic strain in the Apennines from historical earthquakes, *Ann. Geofisc.* **41,** 241–251.

Serpelloni, E., M. Anzidei, P. Baldi, G. Casula, and A. Galvani (2005). Crustal velocity and strain-rate fields in Italy and surrounding regions: New results from the analysis of permanent and nonpermanent GPS networks, *Geophys. J. Int.* **161,** 861–880, doi: 10.1111/j.1365-246X.2005.02618.x.

Templeton, E. L., and J. R. Rice (2008). Off-fault plasticity and earthquake rupture dynamics: 1. Dry materials or neglect of fluid pressure changes, *J. Geophys. Res.* **113,** B09306, doi: 10.1029/2007JB005529.

Terakawa, T., A. Zoporowski, B. Galvan, and S. Miller (2010). High pressure fluid at hypocentral depths in the L'Aquila region inferred from earthquake focal mechanism, *Geology* **38,** 995–998, doi: 10.1130/G31457.1.

Vallée, M. (2004). Stabilizing the empirical Green function analysis: Development of the projected Landweber method, *Bull. Seismol. Soc. Am.* **94,** 394–409.

Vallée, M., J. Charléty, A. M. G. Ferreira, B. Delouis, and J. Vergoz (2011). SCARDEC: A new technique for the rapid determination of seismic moment magnitude, focal mechanism and source time functions for large earthquakes using body wave deconvolution, *Geophys. J. Int.* **184,** 338–358.

Viesca, R. C., E. L. Templeton, and J. R. Rice (2008). Off-fault plasticity and earthquake rupture dynamics: 2. Effects of fluid saturation, *J. Geophys. Res.* **113,** B09307, doi: 10.1029/2007JB005530.

Walters, R. J., J. R. Elliott, N. D'Agostino, P. C. England, I. Hunstad, J. A. Jackson, B. Parsons, R. J. Phillips, and G. Roberts (2009). The 2009 L'Aquila earthquake (central Italy): A source mechanism and implications for seismic hazard, *Geophys. Res. Lett.* **36,** L17312, doi: 10.1029/2009GL039337.

Yano, T. E., G. Shao, Q. Liu, C. Ji, and R. J. Archuleta (2009). Finite fault kinematic rupture model of the 2009 M_w 6.3 L'Aquila earthquake from inversion of strong motion, GPS and lnSAR data, *AGU, Fall Meeting 2009*, Abstract S34A-02.

Zaccarelli, L., N. M. Shapiro, L. Faenza, G. Soldati, and A. Michelini (2011). Variation of crustal elastic properties during the 2009 L'Aquila earthquake inferred from cross-correlation of ambient seismic noise, *Geophys. Res. Lett.* **38,** L24304, doi: 10.1029/2011GL049750.

Dipartimento di Scienze Fisiche
Università degli Studi di Napoli Federico II
Complesso Universitario Monte S. Angelo
via Cintia, 80126 Napoli, Italy
antonella.orefice@na.infn.it
(A.O., A.Z.)

Géoazur-Observatoire de la Côte d'Azur
Centre National de la Recherche Scientifique-Université
de Nice Sophia Antipolis
250, Rue Albert Einstein
06560 Valbonne, France
(M.V., J.B., B.D.)

Manuscript received 12 August 2012